

# FreqBlender: Enhancing DeepFake Detection by Blending Frequency Knowledge

Hanzhe Li<sup>1</sup>, Yuezun Li<sup>1,\*</sup>, Jiaran Zhou<sup>1</sup>, Bin Li<sup>2</sup>, Junyu Dong<sup>1</sup>

<sup>1</sup> College of Computer Science and Technology,  
Ocean University of China, Qingdao, China

<sup>2</sup> Guangdong Key Laboratory of Intelligent Information Processing,  
Shenzhen Key Laboratory of Media Security,  
Shenzhen University, Shenzhen 518060, China

lhzcodes@gmail.com libin@szu.edu.com {zhoujiaran, dongjunyu, liyuezun}@ouc.edu.cn

## Abstract

Generating synthetic fake faces, known as pseudo-fake faces, is an effective way to improve the generalization of DeepFake detection. Existing methods typically generate these faces by blending real or fake faces in color space. While these methods have shown promise, they overlook the simulation of frequency distribution in pseudo-fake faces, limiting the learning of generic forgery traces in-depth. To address this, this paper introduces *FreqBlender*, a new method that can generate pseudo-fake faces by blending frequency knowledge. Specifically, we investigate the major frequency components and propose a Frequency Parsing Network to adaptively partition frequency components related to forgery traces. Then we blend this frequency knowledge from fake faces into real faces to generate pseudo-fake faces. Since there is no ground truth for frequency components, we describe a dedicated training strategy by leveraging the inner correlations among different frequency knowledge to instruct the learning process. Experimental results demonstrate the effectiveness of our method in enhancing DeepFake detection, making it a potential plug-and-play strategy for other methods.

## 1 Introduction

DeepFake refers to face forgery techniques that can manipulate facial attributes, such as identity, expression, and lip movement [Haliassos *et al.*, 2021]. The recent advancement of deep generative models [He *et al.*, 2021; Perov *et al.*, 2020] has greatly sped up the evolution of DeepFake techniques, enabling the creation of highly realistic and visually imperceptible manipulations. However, the misuse of these techniques can pose serious security concerns [Suwajanakorn *et al.*, 2017], making DeepFake detection more pressing than ever before.

There have been many methods proposed for detecting DeepFakes, showing their effectiveness on public datasets [Rossler *et al.*, 2019; Li *et al.*, 2020b; Dolhansky *et al.*, 2019; Dolhansky *et al.*, 2020; Zhou *et al.*, 2021]. However, with the continuous growth of AI techniques, new types

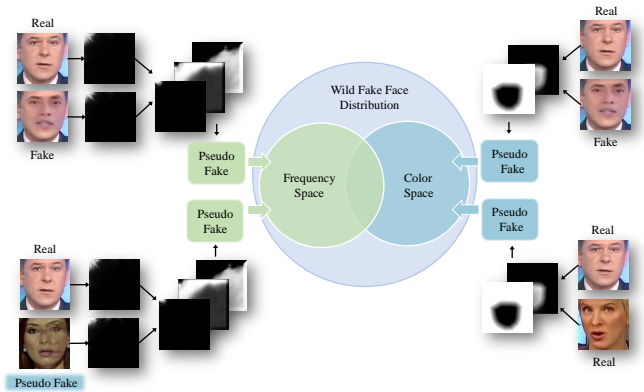


Figure 1: Overview of our method. In contrast to the existing spatial-blending methods (right part), our method explores face blending in frequency space (left part). By leveraging the frequency knowledge, our method can generate pseudo-fake faces that closely resemble the distribution of wild fake faces. Our method can complement and work in conjunction with existing spatial-blending methods.

of forgeries constantly emerge, posing a challenge for current detectors to accurately expose unknown forgeries. To address this challenge, recent efforts [Li and Lyu, 2018; Li *et al.*, 2021; Yan *et al.*, 2023; Wang *et al.*, 2023] have focused on improving the generalizability of detection, *i.e.*, the ability to detect unknown forgeries based on known examples. One effective approach to address this problem is to enhance the training data by generating synthetic fake faces, known as *pseudo-fakes*.

The intuition behind this approach is that the DeepFake generation process introduces artifacts in the step of blending faces, and these methods generate pseudo-fake faces by simulating various blending artifacts. By training on these pseudo-fake faces, the models can be driven to learn corresponding artifacts [Li *et al.*, 2020a; Zhao *et al.*, 2021; Shiohara and Yamasaki, 2022]. However, existing methods concentrate on simulating the *spatial* aspects of face blending. While they can make the pseudo-fake faces resemble the distribution of wild fake faces in color space, they do not explore the distribution in the *frequency space*. Thus, frequency-based forgery clues lack current pseudo-fake faces, limiting the models to learn generic forgery features.

In this paper, we shift our attention from the color space

\*Corresponding author.

to the frequency space and propose a new method called *FreqBlender* to generate pseudo-fake faces by blending frequency knowledge (see Fig. 1). Our idea is to analyze the composition of the frequency space and accurately identify the range of forgery clues falling into. Then we replace this range of real faces with the corresponding range of fake faces to generate pseudo-fake faces. However, it is challenging to obtain the accurate distribution of forgery clues in the frequency space, due to two reasons: 1) the frequency range of forgery clues varies across different fake faces due to its high dependence on face content, and 2) forgery clues may not be concentrated on a single frequency range but could be an aggregation of various portions across multiple ranges. Thus, general low-pass, high-pass, or band-pass filters are incapable of precisely pinpointing the distribution.

To address this challenge, we propose a Frequency Parsing Network (FPNet) that can adaptively partition the frequency space based on the input faces (see Fig. 5). Specifically, we hypothesize that the faces are composed of three frequency knowledge, which represents semantic information, structural information, and noise information, respectively. This hypothesis is validated in our preliminary analysis (refer to Sec. 3 for details). We believe the forgery traces are likely hidden in structural information. Based on this footstone, we design the network consisting of a shared encoder and three decoders to extract corresponding frequency knowledge. The encoder transforms the input data into a latent frequency representation, while the decoders estimate the probability map of the corresponding frequency knowledge.

Training this network is non-trivial since no ground truth of frequency distribution is provided. Therefore, we propose a novel training strategy that leverages the inner correlations among different frequency knowledge. To be specific, we describe dedicated-crafted objectives that are performed on various blending combinations of the output from each decoder and emphasize the properties of each frequency knowledge (see Sec. 4 for details). The experimental results demonstrate that the network successfully parses the desired frequency knowledge within the proposed training strategy.

Once the network is trained, we can parse the frequency component corresponding to the structural information of a fake face, and blend it with a real face to generate a pseudo-fake face. It is important to note that our method is not in conflict with existing spatial blending methods, but rather complements them by addressing the defect in the frequency space. Our method is validated on multiple recent DeepFake datasets (*e.g.*, FF++ [Rossler *et al.*, 2019], CDF [Li *et al.*, 2020b], DFDC [Dolhansky *et al.*, 2020], DFDCP [Dolhansky *et al.*, 2019], FFIW [Zhou *et al.*, 2021]) and compared with many state-of-the-art methods, demonstrating the efficacy of our method in improving detection performance.

The contributions of this paper are summarized in three-fold:

1. To the best of our knowledge, we are the first to generate synthetic fake faces by blending frequency knowledge. Our method makes synthetic fake faces closer to the distribution of wild fake faces, enhancing the learning of generic forgery features in DeepFake detection.

2. We propose a Frequency Parsing Network that can adaptively partition the frequency components corresponding to semantic information, structural information, and noise information, respectively. Since no ground truth is provided, we design dedicated objectives to train this network.
3. Extensive experimental results on several DeepFake datasets demonstrate the efficacy of our method and its potential as a plug-and-play strategy for existing methods.

## 2 Related Works

The rapid progress of AI generative models has spawned the development of DeepFake detection methods. These methods mainly rely on deep neural networks to identify the inconsistency between real and fake faces using various features, including biological signals [Zhou and Lim, 2021], spatial artifacts [Bai *et al.*, 2023; Li *et al.*, 2020a; Zhao *et al.*, 2021; Shiohara and Yamasaki, 2022], frequency abnormality [Wang *et al.*, 2023; Miao *et al.*, 2022; Gu *et al.*, 2022], and the auto-learned clues from dedicated-designed models [Cao *et al.*, 2022; Xu *et al.*, 2023]. These methods have shown promising results on public datasets. However, some of their performance significantly deteriorates when confronted with unknown DeepFake faces due to the large distribution discrepancy resulting from limited training datasets. To tackle this issue, many methods have been proposed to improve their generalizability by learning the generic DeepFake traces, *e.g.*, Face X-ray [Li *et al.*, 2020a], I2G [Zhao *et al.*, 2021], SBI [Shiohara and Yamasaki, 2022]. One effective approach is to generate synthetic fake faces during training, known as pseudo-fake faces. By increasing the diversity of training faces, the gap in the distribution of wild fake faces can be reduced, allowing the models to learn the invariant DeepFake traces across different distributions.

To generate the pseudo-fake faces, recent methods design blending operations to combine different faces. This involves extracting the face region from a source image and blending it into a target image. For instance, DSP-FWA [Li and Lyu, 2018] is a pioneering method that conducts self-blending to simulate fake faces. Several extended variants [Li *et al.*, 2020a; Zhao *et al.*, 2021; Shiohara and Yamasaki, 2022; Chen *et al.*, 2023] have been proposed to blend faces using curated strategies, further improving detection performance.

However, these methods overlook the distribution of wild fake faces in frequency space. While the synthetic faces may resemble the spatial-based distribution, the lack of consideration for frequency perspective hinders the models from learning the fundamental generic DeepFake traces. Therefore, this paper introduces a new method to generate pseudo-fake faces by blending the frequency knowledge, providing a complementary to existing methods.

## 3 Preliminary Analysis

We perform a statistical analysis of the frequency distribution of real and fake faces and present preliminary results for the main frequency components corresponding to semantic information, structural formation, and noise information, respectively.

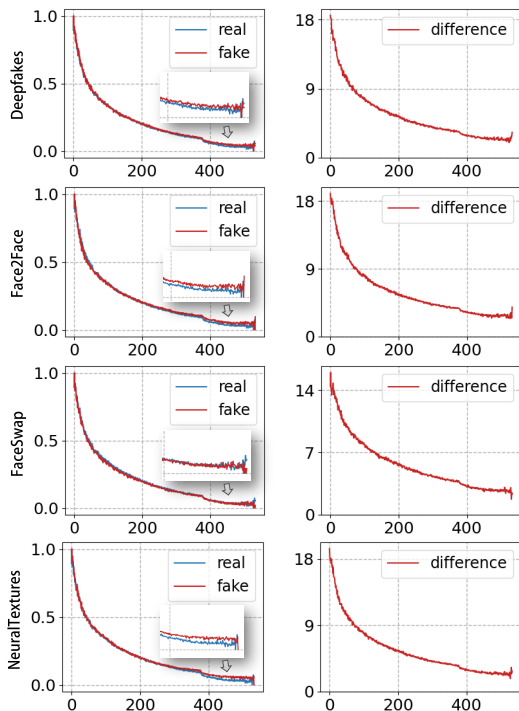


Figure 2: Statistics of frequency distribution. The left part shows the frequency distribution of real and fake faces using algorithms in [Durall *et al.*, 2019; Durall *et al.*, 2020]. The right part shows the frequency difference between real and fake. The values on the vertical axis are logarithmic with 2.

**Inspiration and Verification.** The investigation in previous works [Jia *et al.*, 2022; Durall *et al.*, 2020] has indicated that the forgery traces mainly exist in high-frequency areas. However, the precise range of these areas has not been described, driving us to re-investigate the frequency distribution of forgery traces.

Specifically, we conduct verification experiments using FaceForensics++ (FF++) [Rossler *et al.*, 2019] datasets. We extract the frames from all videos and randomly select 3,000 real images and 3,000 fake images for each manipulation method (*e.g.*, DF, F2F, FS, and NT). Then we crop out the face region in these selected images using a face detector [King, 2009] and apply DCT [Qian *et al.*, 2020] to generate frequency maps. For analysis, we sum up all frequency maps of real and fake images and adopt the visualization process of azimuthal average described in previous work [Durall *et al.*, 2019; Durall *et al.*, 2020]. This process involves logarithmic transformation and the calculation of azimuthally-averaged flux in circular annuli apertures. By placing the center of the circular annuli aperture at the top-left corner of the frequency map, we can obtain a one-dimensional array representing the spectrum diagram. The visual results of their distribution are shown in Fig. 2. It can be observed that this figure is consistent with the results in [Jia *et al.*, 2022]. However, when we directly plot their distribution differences, the results do not match the previous figure. It can be seen that the disparities in high-frequency regions are not as substantial as expected, while the differences in the lower range become more noticeable. This is because the logarithmic operation mitigates

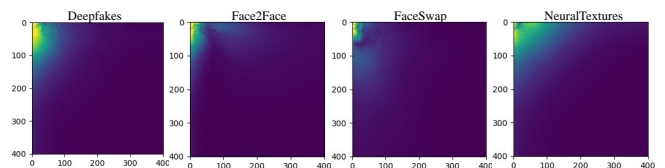


Figure 3: Visualization of the frequency difference between real and fake faces. The lighter color indicates the larger difference.

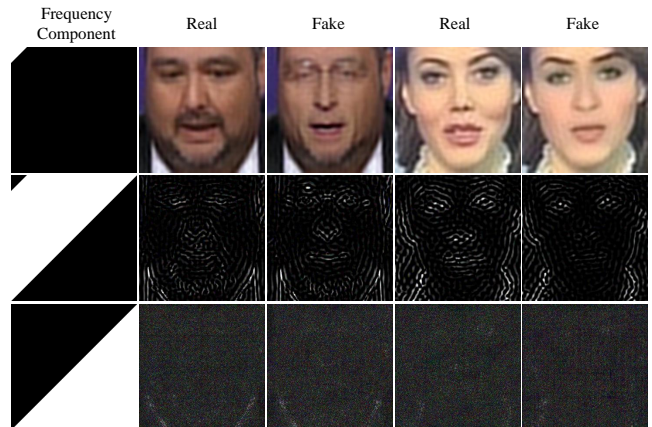


Figure 4: Image visualization corresponding to different frequency components.

the degree of differences in lower frequency ranges, causing the illusion that only the high-frequency range exhibits differences between real and fake faces. Therefore, we conjecture that the forgery traces may not only be concentrated in a very high-frequency range but could possibly extend to the low-frequency range.

**Hypothesis and Validation.** As shown in Fig. 2, the most significant difference can be observed in the range of very low frequency. Given the significant dissimilarity in appearance between real and fake faces, we hypothesize that the semantic information is mainly represented in this low-frequency band. Moreover, we hypothesize that the mid-to-high frequency components capture the structural information, making them more susceptible to containing forgery traces. Furthermore, we hypothesize that the highest frequency components likely correspond to the noise introduced by various video preprocessing operations, such as compression, decompression, and encoding.

To validate our hypothesis, we directly visualize the difference between real and fake faces on their frequency maps in Fig. 3. By observing these results, we empirically split the frequency map into three non-overlap bands. The split operations follow the general band-pass filters. Denote the position in the frequency map as  $(x, y)$ , where  $(0, 0), (1, 1)$  denotes the top-left corner and bottom-right corner. Specifically, we identify the region where  $x + y \leq 1/16$  as containing semantic information, the region where  $1/16 < x + y \leq 1/2$  as containing structural information, and the region where  $x + y > 1/2$  as containing noise information. The corresponding results are visualized in Fig. 4, validating that these three ranges provide empirical evidence that aligns with our frequency distribution hypothesis.

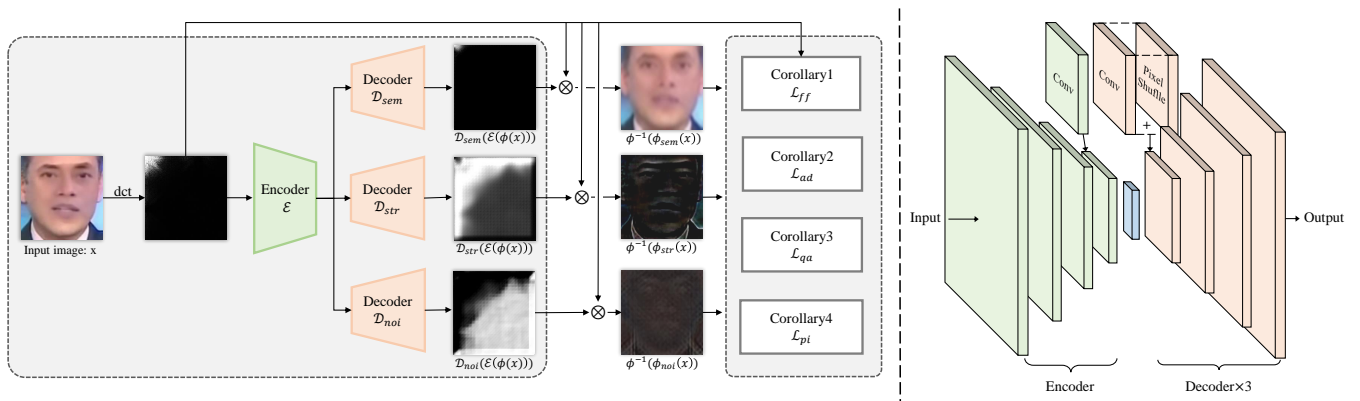


Figure 5: Overview of the proposed Frequency Parsing Network (FPNet). Given an input face image, our method can partition it into three frequency components, corresponding to the semantic information, structural information, and noise information respectively. Since there is no ground truth, we propose four corollaries to supervise the training. The architecture of the encoder and decoders is shown in the right part.

## 4 FreqBlender

We describe a new method to create pseudo-fakes by blending specific frequency knowledge. The motivation is that existing methods only focus on color space blending, which overlooks the disparity between real and fake faces in the frequency space. By considering the frequency distribution, the pseudo-fakes can closely resemble the fake faces. To achieve this, we propose a Frequency Parsing Network (FPNet) to partition the frequency space into three components, corresponding to semantic information, structural information, and noise information, respectively. We then blend the structural information of fake faces with the real faces to generate the pseudo-fakes. The details of the Frequency Parsing Network are elaborated in Sec. 4.1, and the objective and training process for this network is described in Sec. 4.2. Then we introduce the deployment of our method with existing methods in Sec. 4.3.

### 4.1 Frequency Parsing Network

**Overview.** The Frequency Parsing Network (FPNet) is composed of one shared encoder and three independent decoders. The encoder transforms the input faces into frequency-critical features and the decoders aim to decompose the feature from the encoder and extract the respective frequency components.

Denote the encoder as  $\mathcal{E}$  and three decoders as  $\mathcal{D}_{sem}, \mathcal{D}_{str}, \mathcal{D}_{noi}$  respectively. Given an input face image  $\mathbf{x} \in \mathcal{X} \in \{0, 255\}^{h \times w \times 3}$ , we first convert this face to the frequency map as  $\phi(\mathbf{x}) \in \mathbb{R}^{h \times w \times 3}$ , where  $\phi$  denotes the operations of Discrete Cosine Transform (DCT). Then we send this frequency map into model and generate three distribution maps as  $\mathcal{D}_{sem}(\mathcal{E}(\phi(\mathbf{x}))) \in [0, 1]^{h \times w}, \mathcal{D}_{str}(\mathcal{E}(\phi(\mathbf{x}))) \in [0, 1]^{h \times w}$ , and  $\mathcal{D}_{noi}(\mathcal{E}(\phi(\mathbf{x}))) \in [0, 1]^{h \times w}$  respectively. Each distribution map indicates the probability of the corresponding frequency component distributed in the frequency map. Given these distribution maps, we can select the corresponding frequency components conveniently. For example, the frequency component corresponding to semantic information can be selected by  $\phi_{sem}(\mathbf{x}) = \phi(\mathbf{x})\mathcal{D}_{sem}(\mathcal{E}(\phi(\mathbf{x})))$  and the same is for other two frequency components, *i.e.*,  $\phi_{str}(\mathbf{x}) = \phi(\mathbf{x})\mathcal{D}_{str}(\mathcal{E}(\phi(\mathbf{x})))$  and  $\phi_{noi}(\mathbf{x}) = \phi(\mathbf{x})\mathcal{D}_{noi}(\mathcal{E}(\phi(\mathbf{x})))$ . The overview of FPNet is shown in Fig. 5 (left).

**Network Architecture.** The encoder simply consists of four

convolution layers with a kernel size of  $3 \times 3$ , a stride of 2, and a padding of 1. Each decoder also consists of four layers, and each layer is a combination of a convolutional layer and PixelShuffle operation [Shi *et al.*, 2016] (see Fig. 5 (right)).

### 4.2 Objectives for Training Frequency Parsing Network

The most challenging and crucial aspect of our method is training the network for frequency parsing, as there is no ground truth available for the different frequency components.

It is noteworthy that the only available resources for supervision in training are the results of our preliminary analysis in Section 3. However, these results are not accurate and adaptive to different inputs, which is insufficient for the training of the model. Therefore, we meticulously craft a couple of auxiliary objectives to instruct the learning of networks, allowing for the self-refinement of the network.

These objectives are designed based on the following proposition.

**Proposition 1.** *Each frequency component exhibits the following properties:*

1. *Semantic information can reflect the facial identity.*
2. *Structural information serves as the carrier of forgery traces.*
3. *Noise information has minimal impact on visual quality.*
4. *The preliminary analysis findings are generally applicable.*

**Corollary 1.** *For a given face  $\mathbf{x}$ , the transformed face based on its semantic information will retain the same facial identity as  $\mathbf{x}$ , *i.e.*,  $\forall \mathbf{x} \in \mathcal{X} \in \{0, 255\}^{h \times w \times 3}, \mathcal{F}(\phi^{-1}(\phi_{sem}(\mathbf{x}))) = \mathcal{F}(\mathbf{x})$ , where  $\mathcal{F}$  denotes a face recognition model and  $\phi^{-1}$  denotes the Inverse Discrete Cosine Transform (IDCT).*

**Facial Fidelity Loss.** We introduce a facial fidelity loss  $\mathcal{L}_{fid}$  to penalize the discrepancy in identity between the input face image and the spatial content represented by semantic information. To measure the identity discrepancy, we employ

the MobileNet [Howard *et al.*, 2017] as our face recognition model and train it using ArcFace [Deng *et al.*, 2021; Liang *et al.*, 2022]. We select MobileNet for its balance between computational efficiency and recognition accuracy. Let  $\mathcal{F}$  be the MobileNet and  $\mathcal{F}_f(\mathbf{x})$  be the facial features extracted from the face image  $\mathbf{x}$ . The facial fidelity loss can be defined as

$$\mathcal{L}_{\text{ff}}(\mathbf{x}) = \|\mathcal{F}_f(\phi^{-1}(\phi_{\text{sem}}(\mathbf{x}))) - \mathcal{F}_f(\mathbf{x})\|_2^2. \quad (1)$$

Note that the input face  $\mathbf{x}$  can be either real or fake, as the identity information is present in both cases.

**Corollary 2.** *For a given real face  $\mathbf{x}_r$ , it can be detected as fake if and only if it is inserted the structural information from a fake face  $\mathbf{x}_f$ , i.e.,  $\mathcal{D}(\mathbf{x}_r) = 0$  iff  $\mathbf{x}_r \leftarrow \mathbf{x}_r \oplus \phi_{\text{str}}(\mathbf{x}_f)$ , where  $\mathcal{D}$  denotes a Deepfake detector with labels of fake and real in  $\{0, 1\}$ ,  $\oplus$  indicates the inserting operation.*

**Authenticity-determinative Loss.** This loss is designed to emphasize the determinative role of structural information. To evaluate the authenticity of faces, we develop a DeepFake detector  $\mathcal{D}$ , which is implemented using a ResNet-34 [He *et al.*, 2016] trained on real and fake faces. Then we construct two sets of faces by blending frequency components.

The first set contains three types of faces transformed from frequency components corresponding to 1) the semantic information of the real face, 2) the semantic information of the fake face, and 3) the semantic information of the real face blended with the structural information of the fake face. We denote this set as  $\mathcal{C}_r = \{\phi^{-1}(\phi_{\text{sem}}(\mathbf{x}_r)), \phi^{-1}(\phi_{\text{sem}}(\mathbf{x}_f)), \phi^{-1}(\phi_{\text{sem}}(\mathbf{x}_r) + \phi_{\text{str}}(\mathbf{x}_f))\}$ . Since there is no structural information from fake faces in this set, all the faces should be detected as real.

Similarly, the second set contains two types of faces: 1) blending the semantic information of the fake face with the structural information of the fake face, and 2) blending the semantic information of the real face with the structural information of the fake face. We denote this set as  $\mathcal{C}_f = \{\phi^{-1}(\phi_{\text{sem}}(\mathbf{x}_f) + \phi_{\text{str}}(\mathbf{x}_f)), \phi^{-1}(\phi_{\text{sem}}(\mathbf{x}_r) + \phi_{\text{str}}(\mathbf{x}_f))\}$ . Since all blended faces in this set contain the structural information of fake faces, they should be detected as fake. Thus the authenticity-determinative loss  $\mathcal{L}_{\text{ad}}$  can be written as

$$\mathcal{L}_{\text{ad}}(\mathbf{x}_r, \mathbf{x}_f) = \frac{1}{|\mathcal{C}_r|} \sum_{\mathbf{x} \in \mathcal{C}_r} \text{CE}(\mathbf{x}, 1) + \frac{1}{|\mathcal{C}_f|} \sum_{\mathbf{x} \in \mathcal{C}_f} \text{CE}(\mathbf{x}, 0) \quad (2)$$

where CE denotes the cross-entropy loss.

**Corollary 3.** *The face should exhibit no visible change if the frequency component of noise information is removed, i.e.,  $\forall \mathbf{x} \in \mathcal{X} \in \{0, 255\}^{h \times w \times 3}$ ,  $\mathbf{x} \approx \mathbf{x} \ominus \phi_{\text{noi}}(\mathbf{x}_f)$ , where  $\ominus$  indicates the removing operation.*

**Quality-agnostic Loss.** As noise information does not contain decisive details for the overall depiction of the image, the face image is expected to be similar to the face image transformed using the frequency components of semantic and structural information. This similarity can be quantified using the quality-agnostic Loss  $\mathcal{L}_{\text{qa}}$ , defined as

$$\mathcal{L}_{\text{qa}}(\mathbf{x}) = \|\mathbf{x} - \phi^{-1}(\phi_{\text{sem}}(\mathbf{x}) + \phi_{\text{str}}(\mathbf{x}))\|_2^2, \quad (3)$$

where the face  $\mathbf{x}$  can be either real or fake.

**Corollary 4.** *Each frequency component is bound by the preliminary results, i.e., there should be no significant deviation between the predicted frequency component and the approximate frequency distribution in preliminary analysis.*

**Prior and Integrity Loss.** According to our analysis in the Preliminary Analysis section, we have an initial understanding of the approximate frequency distribution. Denote the initial frequency maps for semantic, structural, and noise information as  $m_{\text{sem}}, m_{\text{str}}, m_{\text{noi}}$ , respectively. These maps are utilized to accelerate the convergence of the model towards the desired direction. Moreover, we add a constraint on the integrity of their distributions, ensuring that their combination covers all elements of the frequency map. This loss  $\mathcal{L}_{\text{pi}}$  can be expressed as

$$\begin{aligned} \mathcal{L}_{\text{pi}} = & \|\mathcal{D}_{\text{sem}}(\mathcal{E}(\phi(\mathbf{x}))) - m_{\text{sem}}\|_2^2 + \\ & \|\mathcal{D}_{\text{str}}(\mathcal{E}(\phi(\mathbf{x}))) - m_{\text{str}}\|_2^2 + \\ & \|\mathcal{D}_{\text{noi}}(\mathcal{E}(\phi(\mathbf{x}))) - m_{\text{noi}}\|_2^2 + \\ & \|(\mathcal{D}_{\text{sem}}(\mathcal{E}(\phi(\mathbf{x}))) + \mathcal{D}_{\text{str}}(\mathcal{E}(\phi(\mathbf{x})))) + \\ & \mathcal{D}_{\text{noi}}(\mathcal{E}(\phi(\mathbf{x}))) - \mathbf{1}\|_2^2, \end{aligned} \quad (4)$$

where  $\mathbf{1}$  denotes a mask where all the elements in it is 1.

**Overall Objectives.** The overall objectives are the summation of all these loss terms, as

$$\mathcal{L} = \lambda_1 \mathcal{L}_{\text{ff}} + \lambda_2 \mathcal{L}_{\text{ad}} + \lambda_3 \mathcal{L}_{\text{qa}} + \lambda_4 \mathcal{L}_{\text{pi}}, \quad (5)$$

where  $\lambda_1, \lambda_2, \lambda_3, \lambda_4$  are the weights for different loss terms.

### 4.3 Deployment of FreqBlender

Given a fake face  $\mathbf{x}_r$  and a real face  $\mathbf{x}_f$ , we can generate a pseudo-fake face by

$$\begin{aligned} \mathbf{x}'_f = & \phi^{-1}(\phi(\mathbf{x}_r)\mathcal{D}_{\text{sem}}(\mathcal{E}(\phi(\mathbf{x}_f))) + \\ & \phi(\mathbf{x}_f)\mathcal{D}_{\text{str}}(\mathcal{E}(\phi(\mathbf{x}_f))) + \\ & \phi(\mathbf{x}_r)\mathcal{D}_{\text{noi}}(\mathcal{E}(\phi(\mathbf{x}_f)))) . \end{aligned} \quad (6)$$

Note that in our method, it is not necessary to perform the blending using the wild fake faces. Instead, we can tactfully substitute wild fake faces with the pseudo-fake faces generated by existing spatial face blending methods. It allows us to overcome the limitations in the frequency distribution of existing pseudo-fake faces. Moreover, an example of this is shown in the bottom-left corner of Fig. 1.

## 5 Experiments

### 5.1 Experimental Setups

**DataSets.** Our method is evaluated using several standard datasets, including FaceForensics++ [Rossler *et al.*, 2019] (FF++), Celeb-DF (CDF) [Li *et al.*, 2020b], DeepFake Detection Challenge (DFDC) [Dolhansky *et al.*, 2020], DeepFake Detection Challenge Preview (DFDCP) [Dolhansky *et al.*, 2019], and FFIW-10k (FFIW) [Zhou *et al.*, 2021] datasets. Specifically, the FF++ dataset consists of 1000 pristine videos and 4000 manipulated videos corresponding to four different manipulation methods, that are Deepfakes (DF), Face2Face (F2F), FaceSwap (FS), and NeuralTextures

Table 1: The cross-dataset evaluation of different methods. The best and second-best value is highlighted in blue and red.

Method	Input Type	Training Set		Test Set AUC (%)			
		Real	Fake	CDF	DFDC	DFDCP	FFIW
Two-branch (ECCV'20)	Video	✓	✓	76.65	-	-	-
DAM (CVPR'21)	Video	✓	✓	75.3	-	72.8	-
LipForensics (CVPR'21)	Video	✓	✓	82.4	73.50	-	-
FTCN (ICCV'21)	Video	✓	✓	86.9	71.00	74.0	74.47
DSP-FWA (CVPRW'19)	Frame	✓	✓	69.30	-	-	-
Face X-ray (CVPR'20)	Frame	✓	-	-	-	71.15	-
Face X-ray (CVPR'20)	Frame	✓	✓	-	-	80.92	-
LRL (AAAI'21)	Frame	✓	✓	78.26	-	76.53	-
FRDM (CVPR'21)	Frame	✓	✓	79.4	-	79.7	-
PCL+I2G (ICCV'21)	Frame	✓	-	90.03	67.52	74.37	-
DCL (AAAI'22)	Frame	✓	✓	82.30	-	76.71	71.14
SBI* (CVPR'22)	Frame	✓	-	92.94	72.08	85.51	85.99
SBI (CVPR'22)	Frame	✓	-	93.18	72.42	86.15	84.83
<b>FreqBlender (Ours)</b>	Frame	✓	-	<b>94.59</b>	<b>74.59</b>	<b>87.56</b>	<b>86.14</b>

(NT). CDF dataset comprises 590 pristine videos and 5639 high-quality fake videos created from DeepFake alterations of celebrity videos available on YouTube. DFDC is a large-scale deepfake dataset, that consists of 100,000 video clips, and DFDCP is a preview version of DFDC, which is also widely used in evaluation. The FFIW dataset contains 8250 pristine videos and 8250 DeepFake videos with multi-face scenarios. We follow the original training and testing split provided by the datasets for experiments.

**Compared Methods.** Our method is compared with **four** video-based detection methods, including **Two-branch** [Masi *et al.*, 2020], **DAM** [Zhou *et al.*, 2021], **LipForensics** [Haliassos *et al.*, 2021] and **FTCN** [Zheng *et al.*, 2021]. Moreover, we involve **seven** frame-level state-of-the-art methods for comparison, which are **DSP-FWA** [Li and Lyu, 2018], **Face X-ray** [Li *et al.*, 2020a], **LRL** [Chen *et al.*, 2021], **FRDM** [Luo *et al.*, 2021], **PCL** [Zhao *et al.*, 2021], **DCL** [Sun *et al.*, 2022], **SBI** [Shiohara and Yamasaki, 2022] respectively.

**Implementation Details.** We employ the vanilla EfficientNet-b4 [Tan and Le, 2019] as our detection model. In the training stage, the image size is set to  $400 \times 400$ . The batch size is set to 4 and the Adam optimizer is utilized with an initial learning rate of  $1e^{-4}$ . The training epoch is set to 200. During training, we create pseudo-fake faces on-the-fly. We first generate synthetic faces using the spatial-blending method SBI and then decide whether they are blended with real faces using our method with a probability of  $\alpha$ . We set it to 0.2 in the main experiment (More analysis in *Supplementary*). The hyperparameters in the objective function in Eq. (5) are set as follows:  $\lambda_1 = \frac{1}{12}$ ,  $\lambda_2 = 1$ ,  $\lambda_3 = 1e^{-3}$ ,  $\lambda_4 = \frac{1}{4}$ . In both the training and testing phases, we randomly select 8 frames from each video following [Shiohara and Yamasaki, 2022].

## 5.2 Results

To showcase the effectiveness of our method, we train our method solely on the FF++ dataset and test it on the other different datasets. Following previous works [Shiohara and Yamasaki, 2022; Bai *et al.*, 2023], we employ the frame-level

Area Under the Receiver Operating Characteristic Curve (AUC) as the evaluation metric.

**Cross-dataset Evaluation.** We evaluate the cross-dataset performance of our method compared to other counterparts in Table.1. The best performance is highlighted in blue and the second-best is marked by red. It should be noted that our method operates on pseudo-fake faces generated by SBI, thus we do not need fake faces. In comparison to video-level methods, our method achieves the best performance, which outperforms all the methods by a large margin. Specifically, our method surpasses the most state-of-art method FTCN by 7.69%, 3.59%, 14.41%, 11.67% on CDF, DFDC, DFDCP, FFIW datasets respectively.

When compared to frame-level methods, our method still outperforms the others. For example, our method improves upon the performance of the most state-of-the-art method SBI by 1.41%, 2.17%, 1.41%, 1.31% on CDF, DFDC, DFDCP, FFIW respectively. This improvement can be attributed to the incorporation of frequency knowledge in pseudo-fake faces, enhancing the generalization of detection models. Note that SBI\* denotes the performance obtained using the officially released codes. The results closely align with the reported scores, which verifies the correctness of our configuration of their codes. In subsequent experiments, we employ their release codes for comparison.

**Cross-manipulation Evaluation.** Since SBI is the most recent and effective method, we compare our method with it for demonstration. Specifically, we compare our method with two variants of the SBI method. The first is trained using the raw set of real videos in the FF++ dataset, while the second is trained using the c23 set. According to the standard protocols, all methods are tested on c23 videos. The results are shown in Table.2. It can be seen that our method outperforms SBI-raw by 3.31% and SBI-c23 by 3.58%, demonstrating the efficacy of our method on cross-manipulation scenario. **Saliency Visualization.** We employ Grad-CAM [Selvaraju *et al.*, 2020] to visualize the attention of our method compared to SBI on four manipulations in the FF++ dataset. Compared to SBI, our method concentrates more on the structural infor-

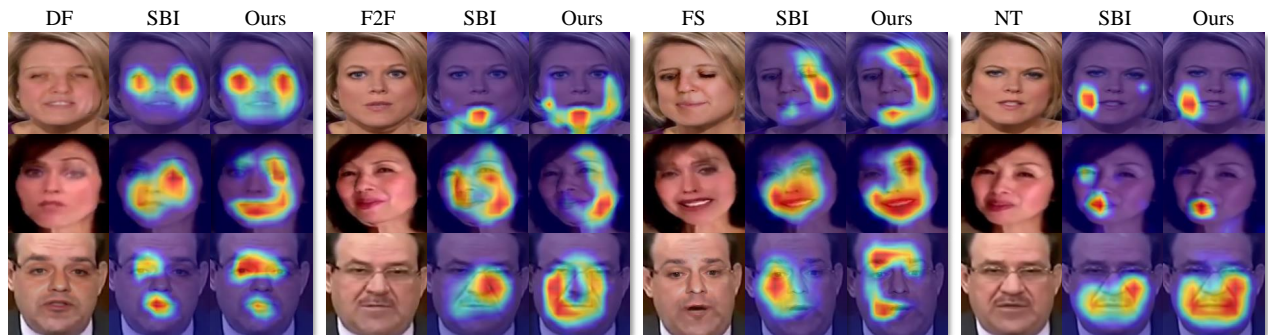


Figure 6: Grad-CAM visualization of SBI and our method on four manipulation types of FF++ dataset. Compared to SBI, our method focuses more on the manipulated structural boundaries.

Table 2: The cross-manipulation evaluation of different methods.

Method	FF++				Avg
	DF	F2F	FS	NT	
SBI-raw	98.35	91.07	96.92	83.69	92.51
SBI-c23	98.60	92.60	95.44	82.30	92.24
<b>FreqBlender (Ours)</b>	99.12	96.64	97.67	89.86	<b>95.82</b>

Table 3: The effect of our method complementary to spatial-blending Methods.

Method	FF++					CDF
	DF	F2F	FS	NT	Avg	
DSP-FWA	55.48	43.79	49.26	44.05	48.14	62.91
DSP-FWA + Ours	56.20	45.93	53.96	41.74	<b>49.46</b>	<b>65.47</b>
I2G	47.83	82.13	60.82	47.47	59.56	<b>53.55</b>
I2G + Ours	56.90	81.26	61.66	55.52	<b>63.84</b>	48.89
Face X-ray	89.38	85.02	83.45	71.17	82.26	67.99
Face X-ray + Ours	93.21	85.41	82.70	74.79	<b>84.03</b>	<b>76.05</b>

mation, such as the manipulation boundaries. For example, our method highlights the face outline in DF, F2F, and FS, while focusing on the mouth contour in NT.

### 5.3 Ablation Study

**Complementary to Spatial-blending Methods.** To validate the complementary of our method, we replace the SBI method with other spatial-blending methods and study if the performance is improved. Specifically, we reproduce the pseudo-fake face generation operations in DSP-FWA, I2G, and Face X-ray, and combine them with our method. Note that I2G and Face X-ray have not released their codes, we reimplement them rigorously following their original settings. The results on FF++ and CDF datasets are presented in Table.4. It can be seen that by combining with DSP-FWA, our method improves 1.31% on FF++ averagely and 2.56% on CDF. A similar trend is also observed in the Face X-ray, which improves 1.78% on average on FF++ and 8.06% on CDF. For I2G, we improve the performance by 4.28% on FF++ but drop on CDF. We attribute it to the ineffective of pseudo-fake faces with less typical traces in frequency space. These results demonstrate that our method can compensate for the lack of frequency knowledge in spatial-blending methods and collaborate with them for improvement.

**Different Network Architectures.** This part validates the effectiveness of our method on different networks, including ResNet-50 [He *et al.*, 2016], EfficientNet-b1 [Tan and Le, 2019], VGG16 [Simonyan and Zisserman, 2014] and Xception [Chollet, 2017]. We compare our method with SBI on these networks, which are tested on CDF, DFDCP, and FFIW

Table 4: The effect of our method on different networks.

Method	CDF	DFDCP	FFIW	Avg
ResNet-50 + SBI	84.82	73.51	81.67	80.00
ResNet-50 + Ours	85.44	76.16	86.32	<b>82.64</b>
EfficientNet-b1 + SBI	90.72	80.45	80.48	83.88
EfficientNet-b1 + Ours	86.99	80.03	88.40	<b>85.14</b>
VGG16 + SBI	78.22	74.13	87.26	<b>79.87</b>
VGG16 + Ours	78.38	73.47	87.63	79.83
Xception + SBI	87.00	75.68	70.24	77.64
Xception + Ours	90.52	76.07	70.43	<b>79.01</b>

Table 5: Ablation study with each objective term.

Setting	CDF	DFDC	DFDCP	FFIW	Avg
Baseline	91.69	72.69	86.67	<b>88.89</b>	84.98
w/o $\mathcal{L}_{ff}$	94.01	74.30	86.86	87.52	85.67
w/o $\mathcal{L}_{ad}$	93.31	72.97	86.32	87.99	85.15
w/o $\mathcal{L}_{qa}$	94.28	74.42	87.25	86.90	85.71
w/o $\mathcal{L}_{pi}$	93.78	74.03	85.99	87.86	85.41
All	<b>94.59</b>	<b>74.59</b>	<b>87.56</b>	86.15	<b>85.72</b>

datasets. The results are shown in Table.4. It can be observed that our method improves the performance by 2.64%, 1.26%, and 1.37% averagely on ResNet-50, EfficientNet-b1, and Xception networks respectively. It is noteworthy that our method slightly reduces the performance of VGG16 by 0.04%. It is possibly because the capacity of VGG16 is limited than other networks, and learning spatial pseudo-fake faces almost fills up this capacity, leaving no room for the learning of frequency knowledge.

**Effect of Each Objective Term.** This part studies the effect of each objective term on CDF and DFDCP datasets. The results are shown in Table.5. Note that Baseline denotes only using prior and integrity loss  $\mathcal{L}_{pi}$  and “w/o” denotes without. It can be seen that without one certain objective term, the performance drops either on the CDF or DFDCP dataset, which demonstrates that different objective terms have distinct impacts, and their collective contributes most to our method.

## 6 Conclusion

This paper describes a new method called *FreqBlender* that can generate pseudo-fake faces by blending frequency knowledge. To achieve this, we propose a Frequency Parsing Network that adaptively extracts the frequency component corresponding to structural information. Then we can blend this information from fake faces into real faces to create pseudo-fake faces. The extensive Experiments demonstrate the effectiveness of our method and can serve as a complementary module for existing spatial-blending methods.

## References

- [Bai *et al.*, 2023] Weiming Bai, Yufan Liu, Zhipeng Zhang, Bing Li, and Weiming Hu. Aunet: Learning relations between action units for face forgery detection. In *Proceedings of the IEEE/CVF Conference on Computer Vision and Pattern Recognition*, pages 24709–24719, 2023.
- [Cao *et al.*, 2022] Junyi Cao, Chao Ma, Taiping Yao, Shen Chen, Shouhong Ding, and Xiaokang Yang. End-to-end reconstruction-classification learning for face forgery detection. In *Proceedings of the IEEE/CVF Conference on Computer Vision and Pattern Recognition*, pages 4113–4122, 2022.
- [Chen *et al.*, 2021] Shen Chen, Taiping Yao, Yang Chen, Shouhong Ding, Jilin Li, and Rongrong Ji. Local relation learning for face forgery detection. In *Proceedings of the AAAI conference on artificial intelligence*, volume 35, pages 1081–1088, 2021.
- [Chen *et al.*, 2023] Han Chen, Yuezun Li, Dongdong Lin, Bin Li, and Junqiang Wu. Watching the big artifacts: Exposing deepfake videos via bi-granularity artifacts. *Pattern Recognition*, 135:109179, 2023.
- [Chollet, 2017] François Chollet. Xception: Deep learning with depthwise separable convolutions. In *Proceedings of the IEEE conference on computer vision and pattern recognition*, pages 1251–1258, 2017.
- [Deng *et al.*, 2021] Jiankang Deng, Jia Guo, Jing Yang, Nannan Xue, Irene Cotsia, and Stefanos P Zafeiriou. Arcface: Additive angular margin loss for deep face recognition. *IEEE Transactions on Pattern Analysis and Machine Intelligence*, page 1–1, Jan 2021.
- [Dolhansky *et al.*, 2019] Brian Dolhansky, Russ Howes, Ben Pflaum, Nicole Baram, and Cristian Canton Ferrer. The deepfake detection challenge (dfdc) preview dataset. *arXiv preprint arXiv:1910.08854*, 2019.
- [Dolhansky *et al.*, 2020] Brian Dolhansky, Joanna Bitton, Ben Pflaum, Jikuo Lu, Russ Howes, Menglin Wang, and Cristian Canton Ferrer. The deepfake detection challenge (dfdc) dataset. *arXiv preprint arXiv:2006.07397*, 2020.
- [Durall *et al.*, 2019] Ricard Durall, Margret Keuper, Franz-Josef Pfrendt, and Janis Keuper. Unmasking deepfakes with simple features. *arXiv preprint arXiv:1911.00686*, 2019.
- [Durall *et al.*, 2020] Ricard Durall, Margret Keuper, and Janis Keuper. Watch your up-convolution: Cnn based generative deep neural networks are failing to reproduce spectral distributions. In *Proceedings of the IEEE/CVF conference on computer vision and pattern recognition*, pages 7890–7899, 2020.
- [Gu *et al.*, 2022] Qiqi Gu, Shen Chen, Taiping Yao, Yang Chen, Shouhong Ding, and Ran Yi. Exploiting fine-grained face forgery clues via progressive enhancement learning. In *Proceedings of the AAAI Conference on Artificial Intelligence*, volume 36, pages 735–743, 2022.
- [Haliassos *et al.*, 2021] Alexandros Haliassos, Konstantinos Vougioukas, Stavros Petridis, and Maja Pantic. Lips don’t lie: A generalisable and robust approach to face forgery detection. In *Proceedings of the IEEE/CVF Conference on Computer Vision and Pattern Recognition*, pages 5039–5049, 2021.
- [He *et al.*, 2016] Kaiming He, Xiangyu Zhang, Shaoqing Ren, and Jian Sun. Deep residual learning for image recognition. In *2016 IEEE Conference on Computer Vision and Pattern Recognition (CVPR)*, Jun 2016.
- [He *et al.*, 2021] Yanan He, Bei Gan, Siyu Chen, Yichun Zhou, Guojun Yin, Luchuan Song, Lu Sheng, Jing Shao, and Ziwei Liu. Forgerynet: A versatile benchmark for comprehensive forgery analysis. *arXiv preprint arXiv:2103.05630*, 2021.
- [Howard *et al.*, 2017] Andrew Howard, Menglong Zhu, Bin Chen, Dmitry Kalenichenko, Weijun Wang, Tobias Weyand, Marco Andreetto, and Hartwig Adam. Mobilenets: Efficient convolutional neural networks for mobile vision applications. *arXiv: Computer Vision and Pattern Recognition*, arXiv: Computer Vision and Pattern Recognition, Apr 2017.
- [Jia *et al.*, 2022] Shuai Jia, Chao Ma, Taiping Yao, Bangjie Yin, Shouhong Ding, and Xiaokang Yang. Exploring frequency adversarial attacks for face forgery detection. In *Proceedings of the IEEE/CVF Conference on Computer Vision and Pattern Recognition*, pages 4103–4112, 2022.
- [King, 2009] Davis King. Dlib-ml: A machine learning toolkit. *Journal of Machine Learning Research*, *Journal of Machine Learning Research*, Dec 2009.
- [Li and Lyu, 2018] Yuezun Li and Siwei Lyu. Exposing deepfake videos by detecting face warping artifacts. *arXiv preprint arXiv:1811.00656*, 2018.
- [Li *et al.*, 2020a] Lingzhi Li, Jianmin Bao, Ting Zhang, Hao Yang, Dong Chen, Fang Wen, and Baining Guo. Face x-ray for more general face forgery detection. In *Proceedings of the IEEE/CVF conference on computer vision and pattern recognition*, pages 5001–5010, 2020.
- [Li *et al.*, 2020b] Yuezun Li, Xin Yang, Pu Sun, Honggang Qi, and Siwei Lyu. Celeb-df: A large-scale challenging dataset for deepfake forensics. In *Proceedings of the IEEE/CVF conference on computer vision and pattern recognition*, pages 3207–3216, 2020.
- [Li *et al.*, 2021] Jiaming Li, Hongtao Xie, Jiahong Li, Zhongyuan Wang, and Yongdong Zhang. Frequency-aware discriminative feature learning supervised by single-center loss for face forgery detection. In *Proceedings of the IEEE/CVF conference on computer vision and pattern recognition*, pages 6458–6467, 2021.
- [Liang *et al.*, 2022] Jiahao Liang, Huafeng Shi, and Weihong Deng. Exploring disentangled content information for face forgery detection. Jul 2022.
- [Luo *et al.*, 2021] Yuchen Luo, Yong Zhang, Junchi Yan, and Wei Liu. Generalizing face forgery detection with high-frequency features. In *Proceedings of the IEEE/CVF conference on computer vision and pattern recognition*, pages 16317–16326, 2021.

- [Masi *et al.*, 2020] Iacopo Masi, Aditya Killekar, Royston Marian Mascarenhas, Shenoy Pratik Gurudatt, and Wael AbdAlmageed. *Two-branch Recurrent Network for Isolating Deepfakes in Videos*, page 667–684. Jan 2020.
- [Miao *et al.*, 2022] Changtao Miao, Zichang Tan, Qi Chu, Nenghai Yu, and Guodong Guo. Hierarchical frequency-assisted interactive networks for face manipulation detection. *IEEE Transactions on Information Forensics and Security*, 17:3008–3021, 2022.
- [Perov *et al.*, 2020] Ivan Perov, Daiheng Gao, Nikolay Chervoniy, Kunlin Liu, Sugasa Marangonda, Chris Umé, Mr Dpfks, Carl Shift Facenheimer, Luis RP, Jian Jiang, et al. Deepfacelab: Integrated, flexible and extensible face-swapping framework. *arXiv preprint arXiv:2005.05535*, 2020.
- [Qian *et al.*, 2020] Yuyang Qian, Guojun Yin, Lu Sheng, Zixuan Chen, and Jing Shao. *Thinking in Frequency: Face Forgery Detection by Mining Frequency-aware Clues*, page 86–103. Jan 2020.
- [Rossler *et al.*, 2019] Andreas Rossler, Davide Cozzolino, Luisa Verdoliva, Christian Riess, Justus Thies, and Matthias Nießner. Faceforensics++: Learning to detect manipulated facial images. In *Proceedings of the IEEE/CVF international conference on computer vision*, pages 1–11, 2019.
- [Selvaraju *et al.*, 2020] Ramprasaath R. Selvaraju, Michael Cogswell, Abhishek Das, Ramakrishna Vedantam, Devi Parikh, and Dhruv Batra. Grad-cam: Visual explanations from deep networks via gradient-based localization. *International Journal of Computer Vision*, page 336–359, Feb 2020.
- [Shi *et al.*, 2016] Wenzhe Shi, Jose Caballero, Ferenc Huszár, Johannes Totz, Andrew P Aitken, Rob Bishop, Daniel Rueckert, and Zehan Wang. Real-time single image and video super-resolution using an efficient sub-pixel convolutional neural network. In *Proceedings of the IEEE conference on computer vision and pattern recognition*, pages 1874–1883, 2016.
- [Shiohara and Yamasaki, 2022] Kaede Shiohara and Toshihiko Yamasaki. Detecting deepfakes with self-blended images. In *Proceedings of the IEEE/CVF Conference on Computer Vision and Pattern Recognition*, pages 18720–18729, 2022.
- [Simonyan and Zisserman, 2014] Karen Simonyan and Andrew Zisserman. Very deep convolutional networks for large-scale image recognition. *arXiv preprint arXiv:1409.1556*, 2014.
- [Sun *et al.*, 2022] Ke Sun, Taiping Yao, Shen Chen, Shouhong Ding, Jilin Li, and Rongrong Ji. Dual contrastive learning for general face forgery detection. In *Proceedings of the AAAI Conference on Artificial Intelligence*, volume 36, pages 2316–2324, 2022.
- [Suwajanakorn *et al.*, 2017] Supasorn Suwajanakorn, Steven M Seitz, and Ira Kemelmacher-Shlizerman. Synthesizing obama: learning lip sync from audio. *ACM Transactions on Graphics (ToG)*, 36(4):1–13, 2017.
- [Tan and Le, 2019] Mingxing Tan and QuocV. Le. Efficient-net: Rethinking model scaling for convolutional neural networks. May 2019.
- [Wang *et al.*, 2023] Yuan Wang, Kun Yu, Chen Chen, Xiyuan Hu, and Silong Peng. Dynamic graph learning with content-guided spatial-frequency relation reasoning for deepfake detection. In *Proceedings of the IEEE/CVF Conference on Computer Vision and Pattern Recognition*, pages 7278–7287, 2023.
- [Xu *et al.*, 2023] Yuting Xu, Jian Liang, Gengyun Jia, Ziming Yang, Yanhao Zhang, and Ran He. Tall: Thumbnail layout for deepfake video detection. In *Proceedings of the IEEE/CVF International Conference on Computer Vision*, pages 22658–22668, 2023.
- [Yan *et al.*, 2023] Zhiyuan Yan, Yong Zhang, Yanbo Fan, and Baoyuan Wu. Ucf: Uncovering common features for generalizable deepfake detection. *arXiv preprint arXiv:2304.13949*, 2023.
- [Zhao *et al.*, 2021] Tianchen Zhao, Xiang Xu, Mingze Xu, Hui Ding, Yuanjun Xiong, and Wei Xia. Learning self-consistency for deepfake detection. In *Proceedings of the IEEE/CVF international conference on computer vision*, pages 15023–15033, 2021.
- [Zheng *et al.*, 2021] Yinglin Zheng, Jianmin Bao, Dong Chen, Ming Zeng, and Fang Wen. Exploring temporal coherence for more general video face forgery detection. In *Proceedings of the IEEE/CVF international conference on computer vision*, pages 15044–15054, 2021.
- [Zhou and Lim, 2021] Yipin Zhou and Ser-Nam Lim. Joint audio-visual deepfake detection. In *Proceedings of the IEEE/CVF International Conference on Computer Vision*, pages 14800–14809, 2021.
- [Zhou *et al.*, 2021] Tianfei Zhou, Wenguan Wang, Zhiyuan Liang, and Jianbing Shen. Face forensics in the wild. In *Proceedings of the IEEE/CVF conference on computer vision and pattern recognition*, pages 5778–5788, 2021.